Journal of Non-Crystalline Solids 513 (2019) 183–190

Contents lists available at ScienceDirect

Journal of Non-Crystalline Solids

journal homepage: www.elsevier.com/locate/jnoncrysol

Structure of TeO_2 glass: Results from 2D ^{125}Te NMR spectroscopy

Maxwell A.T. Marple[a,1], Martha Jesuit[b], Ivan Hung[c], Zhehong Gan[c], Steve Feller[b], Sabyasachi Sen[a,*]

[a] Department of Materials Science & Engineering, University of California at Davis, Davis, CA 95616, United States
[b] Department of Physics, Coe College, Cedar Rapids, IA 52402, United States
[c] Center for Interdisciplinary Magnetic Resonance, National High Magnetic Field Laboratory, 1800 East Paul Dirac Drive, Tallahassee, FL 32310, United States

ARTICLE INFO

Keywords:
TeO2 glass structure
Two-dimensional ^{125}Te NMR
Isotropicanisotropic chemical shift correlation
Te-O coordination
Raman spectroscopy

ABSTRACT

Despite its chemical simplicity, a definitive description of the structure of TeO_2 glass has remained elusive due to the complexity of the Te-O coordination environment. In this work we probe the Te-O coordination environment in glassy TeO_2 using 2D ^{125}Te isotropic-anisotropic chemical shift correlation nuclear magnetic resonance (NMR) spectroscopy. The NMR results are consistent with the presence of two Te-O environments in this glass, characterized by their distinct set of ^{125}Te chemical shift parameters. The dominant environment (~89%) is a distorted trigonal bipyramidal TeO_4 unit, reminiscent of that observed in crystalline γ-TeO_2. A second, minor (~11%) component can be assigned, on the basis of its chemical shift parameters, to a TeO_3 unit. The resulting average coordination number, n_{TeO}, measured by ^{125}Te NMR ($n_{TeO} \approx 3.9$) is higher than its previously reported value obtained using neutron diffraction ($n_{TeO} \approx 3.7$).

1. Introduction

TeO_2 based glasses are promising materials for non-linear optical devices due to their high refractive index and non-linear optical (NLO) susceptibility, that are some of the highest among oxide glasses [1]. The origin of these optical properties is attributed to the presence of long and weak Te-O bonds and to the lone pair electrons on the Te atoms [2,3]. However, the establishment of structure-property relationships in tellurite glasses has remained challenging, primarily owing to their structural complexity. The nature and variety of the Te-O coordination environments remain poorly understood even in the chemically simplest glass-former TeO_2 [4–6]. Important insight in this regard can be gained from a consideration of the structure of crystalline polymorphs of TeO_2 [7,8]. One of the distinguishing features of tellurite compounds is the stereochemical effect imparted by the lone-pair electrons on Te which results in a strong asymmetry of the Te-O coordination polyhedra. The crystal structure of the polymorph α-TeO_2 consists of corner-sharing TeO_4 trigonal bipyramids with the lone pair electrons occupying one of the corners of the bipyramid (Fig. 1). The central Te atom in this bipyramid has two short (1.88 Å) equatorial bonds (Te-O_{eq}) and two longer (2.12 Å) axial bonds (Te-O_{ax}). In the structure of α-TeO_2 each TeO_4 bipyramid shares its corners through an alternating pattern of equatorial and axial Te-O bonds i.e. through the Te-$_{eq}O_{ax}$-Te bridges. These asymmetric bridges play an important role in the structural arrangements of the Te-O coordination polyhedra in tellurite compounds. Additionally, the unique charge distribution arising from the asymmetry and the weak Te-O_{ax} bonds is believed to be responsible for the large NLO susceptibility found in TeO_2 [2].

It was originally assumed that the structure of glassy TeO_2 should resemble that of the α-TeO_2, in the sense that the Te-O network is made up of similar TeO_4 bipyramidal units, except with a distribution of lengths for the axial and equatorial Te-O bonds. However, since the discovery of the metastable polymorph γ-TeO_2, it is now widely believed that the structure of glassy TeO_2 should resemble that of γ-TeO_2, a hypothesis that is corroborated by the similarity in their vibrational spectra and by the observation that γ-TeO_2 crystallizes from TeO_2 glass before the α phase [9,10]. Similar to α-TeO_2, the structure of γ-TeO_2 also contains trigonal bipyramidal Te-O coordination polyhedra, except the Te-O bond lengths of the axial and equatorial bonds in the latter phase are all dissimilar, with the Te-O_{eq} distances being 1.859 and 1.948 Å while the Te-O_{ax} distances are 2.019 and 2.197 Å (Fig. 1). The bipyramidal units in γ-TeO_2 are bridged via Te-$_{eq}O_{ax}$-Te in the same way as α-TeO_2, however, due to the asymmetry of the TeO_4 structural unit, the connectivity alternates between nearly symmetric (1.95–2.02 Å) and asymmetric (1.86–2.20 Å) bridges. Through this discrepancy in Te-O-Te bridges, the symmetrical bridges can be viewed

* Corresponding author.
E-mail address: sbsen@ucdavis.edu (S. Sen).
[1] Current address: Physical and Life Science Directorate, Lawrence Livermore National Laboratory, Livermore, CA 94550, United States.

https://doi.org/10.1016/j.jnoncrysol.2019.03.019
Received 19 December 2018; Received in revised form 6 March 2019; Accepted 11 March 2019
0022-3093/

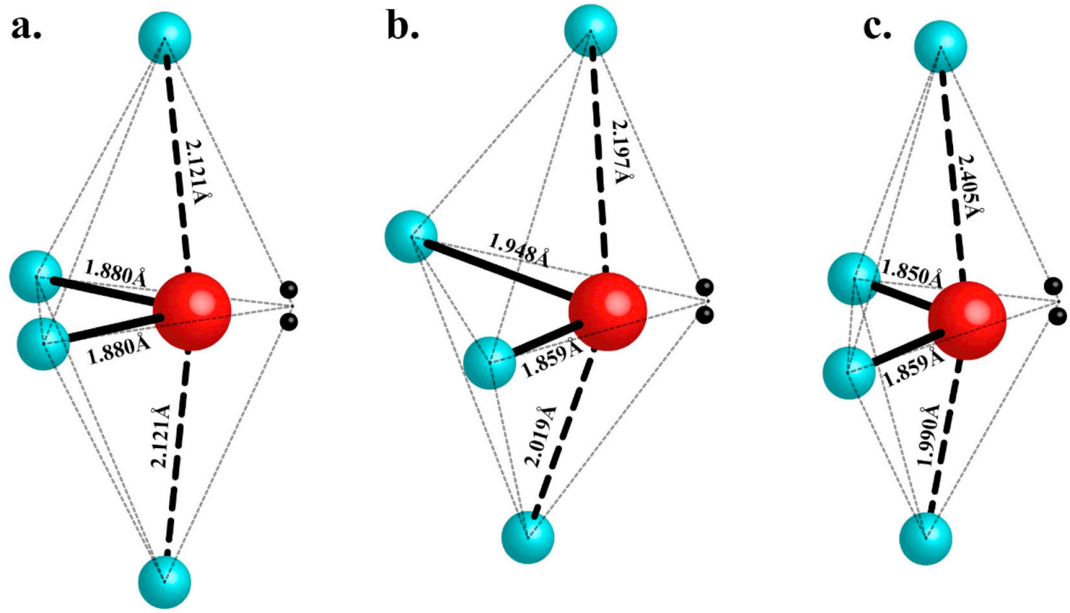

Fig. 1. Schematics of Te-O trigonal bipyramidal coordination polyhedral configuration in: (a) α-TeO_2, (b) γ-TeO_2 and (c) $MgTe_2O_5$. Tellurium atoms are represented in red and Oxygen atoms in blue, with the lone pair electrons by two black spheres. Bold black lines indicate the Te-O_{eq} bonds and bold dashed lines represent Te-O_{ax} bonds. (For interpretation of the references to colour in this figure legend, the reader is referred to the web version of this article.)

as forming a polymeric chain-like structure [8]. In fact, since one of the Te-O_{ax} bonds in γ-TeO_2 is substantially longer (~2.2 Å) than the others, the Te-O polyhedron in this polymorph is occasionally designated as TeO_{3+1} rather than TeO_4. However, more typically the TeO_{3+1} polyhedra in tellurite crystal structures (e.g. $MgTe_2O_5$) are characterized by significantly longer Te-O distances on the order of ~ 2.5 Å.

It should be noted here that the literature on the structure of glassy TeO_2 is relatively scant due to the difficulty in its synthesis as it devitrifies readily without addition of modifiers. Although small batches of pure glassy TeO_2 have been synthesized using controlled quenching [9], most of the structural studies on tellurite compounds and glasses have focused on systems containing modifier cations such as alkalis and alkaline-earths [11–19]. Addition of a modifier cation to TeO_2 acts to reduce the coordination number of Te to 3 and form Te(=O)$O_{2/2}$ type TeO_3 units as well as to break up the Te-O-Te network via creation of non-bridging oxygen (NBO) atoms on the 3- and 4-coordinated Te-O units.

Recent neutron diffraction, Raman spectroscopy and molecular simulation studies have indicated that the structure of TeO_2 glass possibly contains both TeO_4 and TeO_3 units, resulting in an effective Te-O coordination number that is significantly < 4 [4,9,20,21]. Among these studies, the diffraction results are the most quantitative, which yield an average coordination number n_{TeO} ~ 3.7 that is rationalized by proposing that glassy TeO_2 is composed of TeO_4 and Te(=O)$O_{2/2}$ type TeO_3 units, and the presence of the latter units promotes the formation of NBO environments upon addition of modifier. Molecular dynamics simulations have yielded similar n_{TeO} values, however, they predict a distribution of Te-O units with 3, 4, and 5 coordinated Te [20,21]. Additionally, while assignments of the Raman spectra of TeO_2 has been a source of debate, Kalampounias et al. have interpreted certain vibrational modes to be from TeO_3 units and estimated the average coordination number from integrating the corresponding Raman bands [9].

To date there are only a few reports utilizing ^{125}Te solid state nuclear magnetic resonance (NMR) spectroscopy to study the structure of pure glassy TeO_2 [6,14]. Extensive work has recently been done by Garaga et al. [6], which revealed that the static ^{125}Te NMR spectrum of glassy TeO_2 is similar to that of γ-TeO_2 and could be described structurally as a highly disordered form of γ-TeO_2 containing TeO_{3+1} units. Additionally, the ^{17}O NMR results strongly suggest the lack of terminal oxygen and thus, the absence of significant concentration of Te(=O)$O_{2/2}$ type TeO_3 units in the glass. Further interpretation of the static ^{125}Te NMR spectrum is hindered by the rather large broadening effects from both chemical shift distribution and chemical shift anisotropy that is also characteristic of the ^{125}Te NMR spectra of all tellurite compounds. Despite the broadened and often unresolved ^{125}Te NMR line shape (often on the order of 1500 ppm), there are a plethora of ^{125}Te NMR spectroscopic studies that can be found in the literature on crystalline and glassy tellurites, that have been described in terms of the broad ^{125}Te NMR chemical shift systematics of the TeO_4 and TeO_3 units [6,11–15,18,19]. The ^{125}Te resonance of the TeO_3 environment becomes very prominent for the highly modified tellurite glasses. However, conventional 1D ^{125}Te NMR spectroscopy does not offer enough resolution to distinguish whether such environments exist within glassy TeO_2.

Here we report the results of a 2D isotropic anisotropic chemical shift correlation ^{125}Te NMR spectrum of glassy TeO_2 acquired using the projection Magic Angle Turning (*pj*MAT) technique to separate the chemical shift anisotropy (CSA) from the isotropic shift in two dimensions. The CSA-free isotropic spectrum effectively represents a magic-angle-spinning (MAS) spectrum acquired with infinite spinning speed and therefore, is only broadened by isotropic chemical shift distribution. Thus, the isotropic ^{125}Te NMR spectrum has a significantly narrower line shape (~125 kHz) compared to the static line width of ~400 kHz, thus providing enhanced resolution to observe multiple structural units based on their isotropic chemical shifts, with their distinction being further aided by the difference in their CSA that can be obtained from the anisotropic dimension. We demonstrate that this technique offers unique insight into the structural units based on local site symmetry, which is used in an attempt to resolve the long-standing structural issues in glassy TeO_2.

2. Experimental methods

2.1. Synthesis and characterization

Samples of glassy TeO_2 were prepared by melting reagent grade crystalline oxide (Sigma Aldrich, Co.) in a platinum crucible, at 1000 °C for 10 min followed by intermittently quenching the bottom of the crucible in ice-water, a method described in detail in previous publications in the literature [5]. Glassy samples, of about 0.5 g to a few grams, were obtained. These small pieces of yellow-green glasses were easily removed from the crucible.

The amorphous character of the TeO_2 sample was verified by X-ray diffraction using a PANalytical X'PERT PRO diffractometer equipped with a Cu Kα source. The density of the TeO_2 sample was measured using a Micromeritics AccuPyc II gas expansion pycnometer under a helium environment of 6 N purity on about 0.5 g of glass pieces. The reported density is an average of 10 consecutive measurements at 25 °C. The glass transition temperature T_g was determined using differential scanning calorimetry (DSC). The DSC scans were performed with a Mettler-Toledo DSC1 calorimeter. As noted previously by Tagiara et al., pure TeO_2 glass crystallizes readily during a conventional DSC scan and prevents any observation of T_g. However, through a combination of annealing above 100 °C to drive off the moisture and using a fast heating rate, a glass transition can be observed [5]. In the present study T_g was measured on bulk flakes of glass after using the following heat treatment: the glass sample was first heated to 120 °C and held for 40 min, followed by heating to 450 °C at a rate of 40 °C/min.

The unpolarized Raman spectrum of the glass sample was collected using a Bruker RFS 100/S Fourier-transform Raman spectrometer equipped with a frequency doubled Nd:YAG laser operating at 1064 nm. The spectrum was collected in backscattering geometry with a laser power of 50 mW, a frequency resolution of 2 cm^{-1}, and by averaging 256 scans.

2.2. ^{125}Te NMR spectroscopy

The ^{125}Te *pj*MATPASS/CPMG NMR measurement was carried out at the National High Magnetic Field Laboratory on a Bruker Avance III HD console equipped with a 18.8 T medium bore (63 mm) magnet, operating at a ^{125}Te Larmor frequency of 252.4 MHz. Crushed glass powder was packed and spun at 10 kHz in a 3.2 mm ZrO_2 rotor. The *pj*MATPASS/CPMG experiment separates isotropic and anisotropic chemical shift in two dimensions regardless of how large the CSA is, relative to the spinning frequency. The ^{125}Te *pj*MATPASS/CPMG NMR spectrum was acquired using 64 hypercomplex t_1 data points, with 72 transients per point, 320 CPMG echoes per transient, and a recycle delay of 40 s. Fig. 2 shows the *pj*MATPASS/CPMG pulse sequence with its details outlined elsewhere [22]. CPMG echo acquisition was appended to the sequence to enhance the signal to noise and reduce the data collection time. A 2 μs π/2 pulse was used for both the projection pulse and for the CPMG pulse. This pulse length is sufficient to ensure uniform excitation of the whole powder pattern, which spans ~400 kHz. Full-echo processing was employed to avoid any ambiguity in phasing. The ^{125}Te NMR spectrum was referenced to neat $(CH_3)_2Te$ with $\delta_{iso} = 0$ ppm by using the ^{17}O signal of H_2O and the frequency ratios listed for ^{17}O and ^{125}Te in the IUPAC recommendations [23]. The resulting 2D isotropic-anisotropic correlation spectrum was obtained by summation of the CPMG echoes followed by Fourier transformation and shearing along both the F1 and F2 dimensions. The projections along the isotropic and anisotropic dimensions were simulated using the software Dmfit [24]. The principal components of the chemical shift tensor (δ_{xx}, δ_{yy}, and δ_{zz}) are expressed in terms of the isotropic chemical shift δ_{iso}, the magnitude of anisotropy Δ, and the asymmetry parameter η, in accordance with the Haeberlen convention [25]. These parameters are defined as:

$$\delta_{iso} = \frac{1}{3}(\delta_{zz} + \delta_{yy} + \delta_{xx});\ \Delta = \delta_{zz} - (\delta_{xx} + \delta_{yy})/2;\ \eta = \frac{\delta_{yy} - \delta_{xx}}{\delta_{zz} - \delta_{iso.}}$$

where, $\delta_{zz} - \delta_{iso} \geq \delta_{xx} - \delta_{iso} \geq \delta_{yy} - \delta_{iso}$.

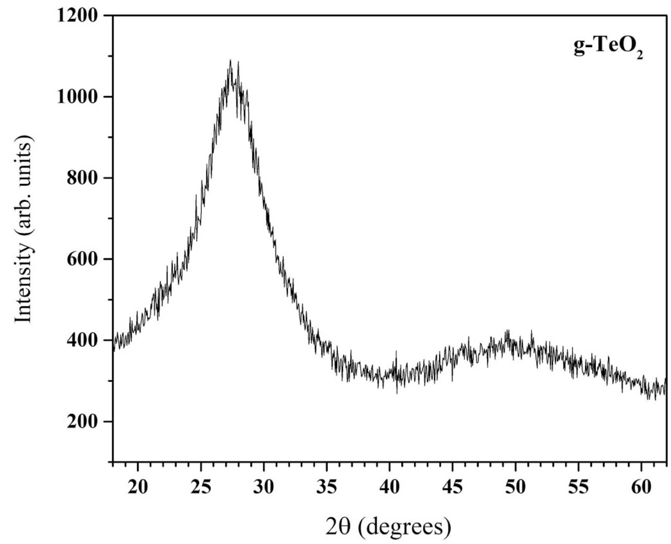

Fig. 3. X-ray diffraction pattern of TeO_2 glass sample used in the present study.

3. Results and discussion

Given the inherent difficulty to synthesize amorphous TeO_2 due to its propensity to crystallize during conventional quenching techniques, it was necessary to verify the glassy character of the sample under study. The XRD pattern of the glass sample used in the present study is shown in Fig. 3, which displays a typical powder pattern for an amorphous sample which is devoid of sharp Bragg peaks corresponding to long-range order. Furthermore, the sample displays a glass transition at ~308 °C and has a density of 5.61 ± 0.01 g/cm^3, both of which are in excellent agreement with previous reports in the literature [5,26]. These measurements indicate the sample is of good quality and can be considered a representative sample of glassy TeO_2 synthesized via the intermittent quenching technique. This conclusion is further corroborated by the Raman spectrum of this sample as shown in Fig. 4, which is virtually identical to those previously published in the literature [6,9]. The high frequency region of this spectrum is decomposed into four bands centered at ~ 617, 660, 715 and 776 cm^{-1} following Kalampounias et al., where the first two bands are assigned to the symmetric stretching modes of TeO_4 trigonal bipyramid units and the last

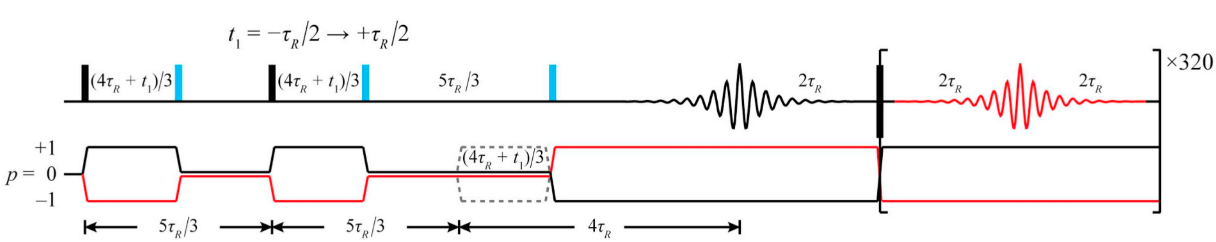

Fig. 2. Schematic of the 2D *pj*MATPASS/CPMG pulse sequence including timing durations used experimentally in this work. A constant delay of $4\tau_R$, where τ_R is the sample spinning period, is introduced in the t_1-evolution for full echo CPMG signal acquisition. The timing of the three t_1-evolution segments is separated by 120° in terms of the rotor phase. For additional information regarding the pulse sequence, please see Ref. 22.

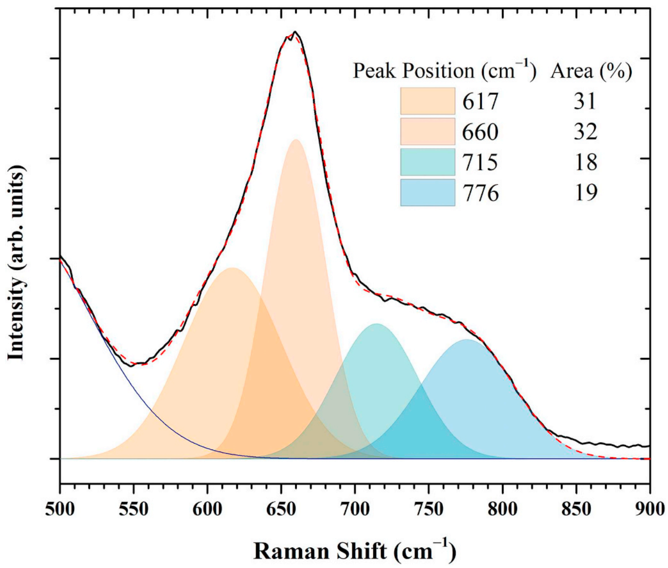

Fig. 4. Unpolarized Raman spectrum of TeO_2 glass sample used in the present study.

two bands correspond to the symmetric stretching modes of TeO_3 trigonal pyramid units [27]. Therefore, assuming that these stretching modes have comparable Raman cross-sections, their relative areas can be used to estimate the average coordination number for Te in glassy TeO_2. This procedure yields $n_{TeO} \approx 3.63$, which agrees well with previous estimates obtained using Raman spectroscopy and neutron diffraction [4,27].

The static ^{125}Te NMR spectrum of glassy TeO_2 was previously reported by Garaga et al. and was interpreted to be composed of a single environment whose ^{125}Te chemical shift tensor can be described by $\delta_{iso} = 1570$ ppm, $\Delta = -1260$ ppm and $\eta = 0.5$ [6]. These authors, however, noted that the spectrum can also be represented equally well by a two-component fit, although the tensor parameters for the two environments could not be uniquely determined.

The 2D ^{125}Te *pj*MATPASS/CPMG NMR spectrum of glassy TeO_2 acquired in the present study and its isotropic projection are shown in Fig. 5. The isotropic spectrum, which is equivalent to an MAS spectrum at infinite spinning speed, is dominated by a broad resonance centered at ~1500 ppm, which if symmetric, suggests the presence of a minor component centered at ~1700 ppm that is manifested as a high-frequency asymmetric tail. Additionally, a third narrow resonance centered at ~1491 ppm can be readily identified, implying that a small fraction of the glass has crystallized. The CSA parameters Δ and η obtained from the simulation of the anisotropic line shapes of these isotropic resonances can provide further information on the local site symmetry of the corresponding Te environments. The representative slices along the anisotropic dimension, taken at the isotropic shifts of 1541 ppm and 1735 ppm (Fig. 5, dashed lines) corresponding to the major and minor Te environments in glassy TeO_2 are shown in Fig. 6. These two isotropic shifts are chosen at first since the major and the minor components will have only little overlap at these two positions and at the same time the anisotropic line shape on the high-frequency side will have enough intensity to provide reliable CSA parameters. It is clear that the anisotropic line shapes for these two Te environments in the glass are different. These anisotropic line shapes can be simulated to determine their CSA parameters Δ and η (Fig. 6). It may be noted that Δ and η denote, respectively, the departure of the chemical shift tensor from spherical and axial symmetry. Both Δ and η for the isotropic shift at 1541 ppm are distinctly larger than that at 1735 ppm and hence, the chemical shift tensor for the latter Te environment is more symmetric compared to the former. Fig. 7 shows the variation of the CSA parameters Δ and η through the entire isotropic line shape, if the anisotropic

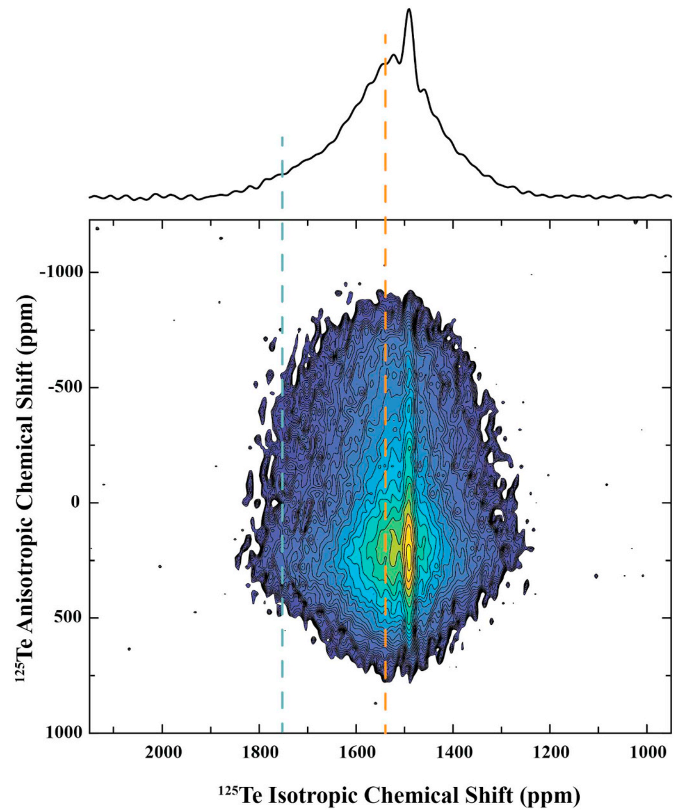

Fig. 5. Contour plot of 2D ^{125}Te *pj*MATPASS/CPMG NMR spectrum of glassy TeO_2. Total isotropic projection of the spectrum is shown on top. The dashed vertical lines indicate the δ_{iso} location for the anisotropic slices shown in Fig. 6.

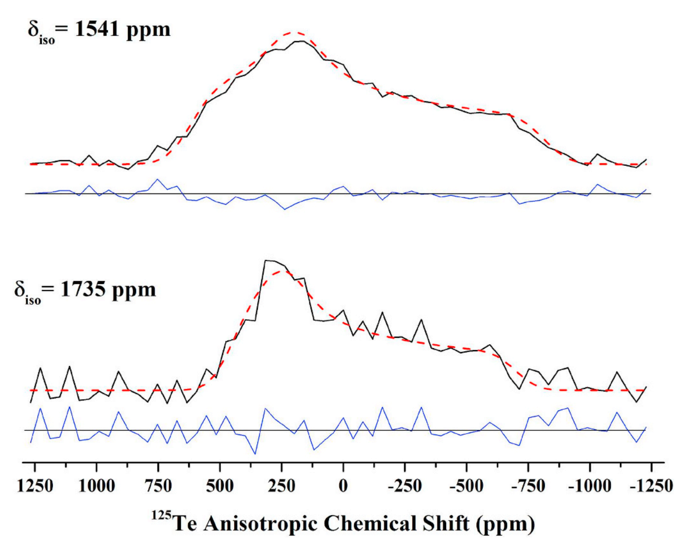

Fig. 6. Experimental (solid line) and simulated (dashed lines) anisotropic ^{125}Te NMR spectral line shapes of glassy TeO_2, taken from the ^{125}Te *pj*MATPASS/CPMG NMR spectrum in Fig. 5 at different δ_{iso} values indicated on the left of each line shape.

line shapes are simulated with a single set of such parameters. At high frequencies ($\delta_{iso} \geq 1715$ ppm), the CSA can be characterized by $\Delta = -1032 \pm 50$ ppm and $\eta = 0.30 \pm 0.05$. With decreasing chemical shift, the magnitude of both Δ and η gradually increase until δ_{iso} ~1600 ppm, at which point the isotropic line shape is dominated by the major Te environment in the glass structure and is characterized by Δ and η of -1215 ± 30 ppm and 0.50 ± 0.03, respectively. These values of Δ and η remain practically unchanged, within error, between

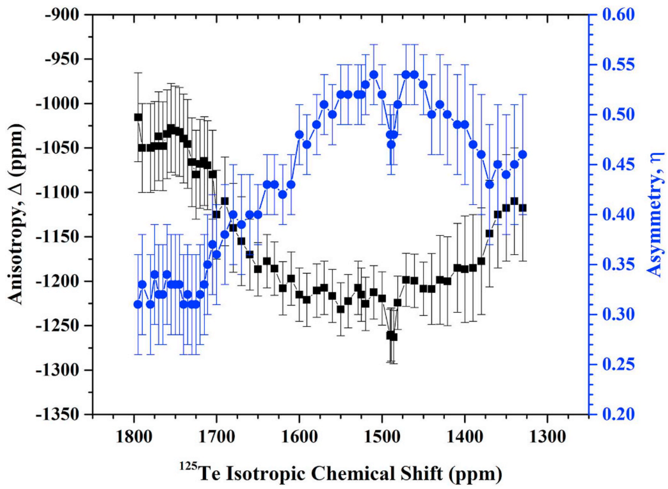

Fig. 7. Variation of anisotropy Δ (black squares) and asymmetry parameter η (blue circles) of the ^{125}Te NMR chemical shift tensor with isotropic chemical shift, as obtained from simulation of each anisotropic line shape with a single set of Δ and η. (For interpretation of the references to colour in this figure legend, the reader is referred to the web version of this article.)

1600 ppm and 1400 ppm and then change to −1125 ± 50 ppm and 0.45 ± 0.05, respectively, between 1400 and 1350 ppm (Fig. 7). The continuous change in Δ and η between ~1600 and 1700 ppm (Fig. 7) suggests significant overlap between the two Te environments, which warrants simulation of the anisotropic line shapes in this region with two components. Examples of such simulations are shown in Fig. 8, which indicate that the anisotropic line shapes in this region can be described well in terms of the two sets of Δ and η parameters that are characteristic of the two Te environments. The corresponding variations of the CSA parameters obtained from these simulations, and the relative contributions of the two Te environments thus obtained, are shown in Fig. 9. Following this line of argument, the isotropic ^{125}Te NMR spectrum can indeed be simulated well with the two glassy and one crystalline environment, as shown in Fig. 9. Furthermore, the relative contributions of the two glassy environments obtained from this fit agree reasonably well with those obtained from the simulations of the anisotropic line shapes (Fig. 9c).

The two glassy Te environments with corresponding resonances centered at 1518 and 1705 ppm are present in a 86:11 ratio and constitute 97% of the isotropic signal, while the crystalline environment makes up for the rest 3% (Fig. 9). The major component at 1518 ppm can be identified as a somewhat distorted TeO_4 trigonal bipyramidal environment as this ^{125}Te δ_{iso} is very close to that of γ-TeO_2, while the

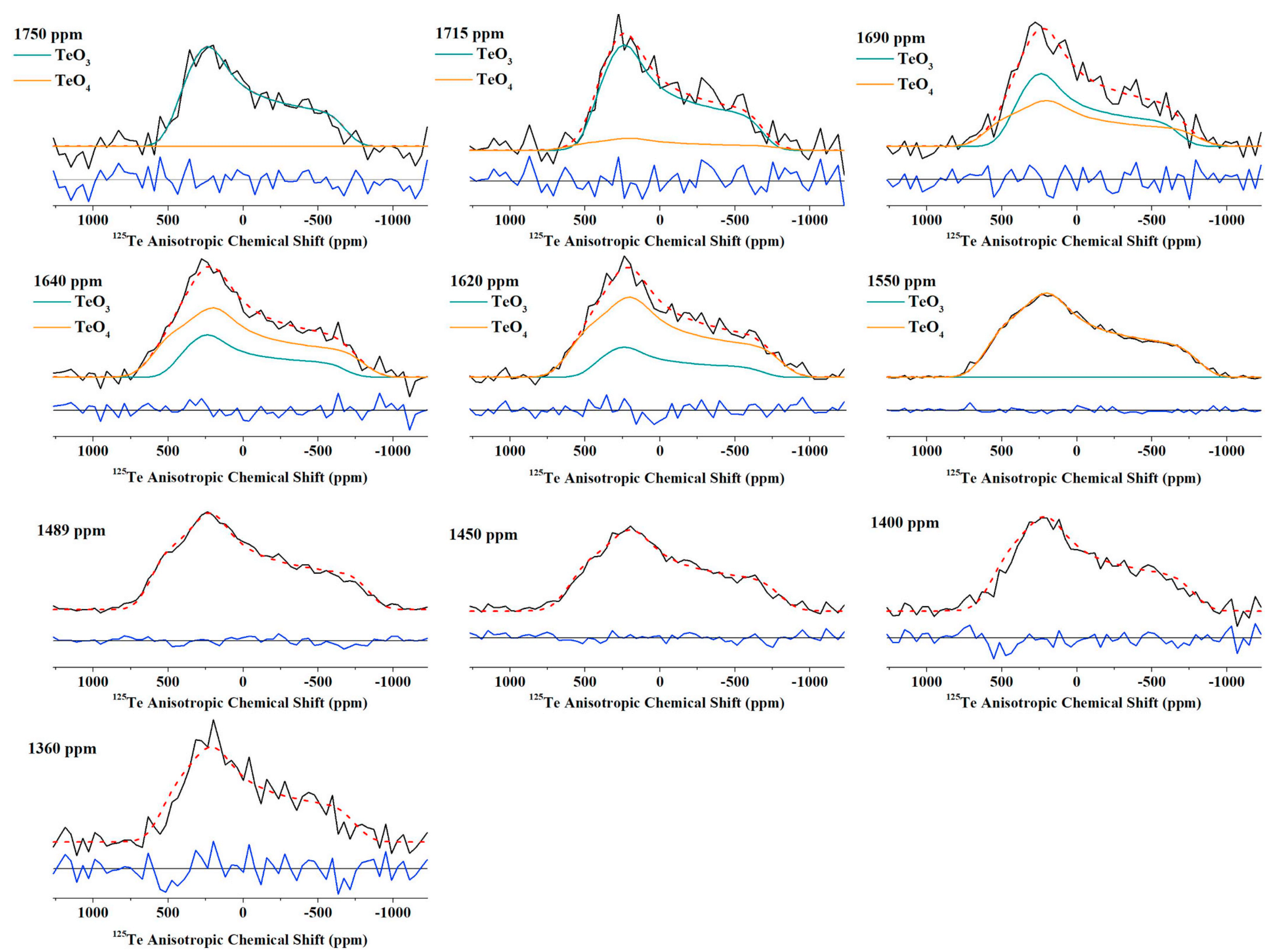

Fig. 8. Experimental (black solid line) and simulated (red dashed lines) anisotropic ^{125}Te NMR spectral line shapes of glassy TeO_2, taken from the ^{125}Te *pj*MATPASS/CPMG NMR spectrum at a series of δ_{iso} values as indicated at the top left corner for each case. For two-component fits, individual simulation components are shown in light orange and teal. Fit residuals are shown as blue lines. (For interpretation of the references to colour in this figure legend, the reader is referred to the web version of this article.)

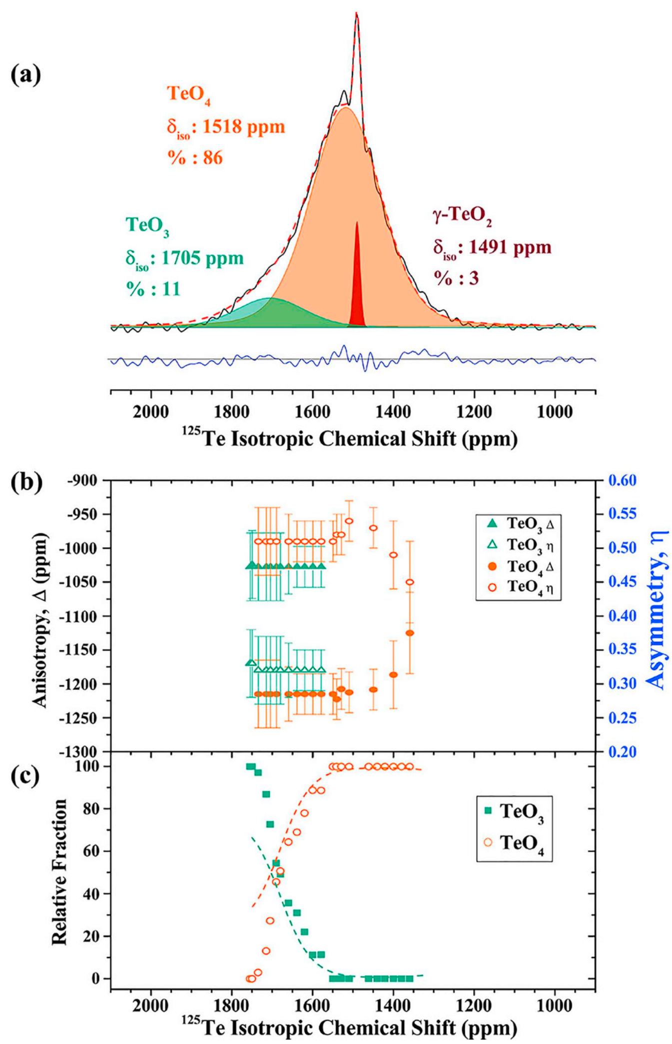

Fig. 9. (a) Experimental (solid line) and simulated (dashed line) ^{125}Te isotropic NMR spectrum of glassy TeO_2. The three constituent simulation components corresponding to γ-TeO_2 crystal, glassy TeO_4 and TeO_3 environments are shown in red, light orange and teal, respectively. The line shapes of glassy components are a mixed Gaussian-Lorentzian (78% Gaussian) while that of the crystal component is 100% Gaussian. (b) Variation of Δ and η with isotropic chemical shift, as obtained from simulations shown in Fig. 8. (c) Relative intensities of glassy TeO_4 and TeO_3 environments obtained from simulation of the isotropic line shape (dashed lines) are compared with those obtained from simulation of anisotropic line shapes (symbols) at various chemical shifts. (For interpretation of the references to colour in this figure legend, the reader is referred to the web version of this article.)

Table 1
Isotropic chemical shift, anisotropy Δ and asymmetry parameter η of crystalline TeO_2 polymorphs and glassy TeO_2 from literature and obtained in the present study. Numbers in parentheses indicate the error.

^{125}Te Environment	δ_{iso} (ppm)	Δ (ppm)	η	Source
α-TeO_2	1469 (2)	−1107 (6)	0.66 (0.02)	Garaga et al. [6]
γ-TeO_2	1509 (10)	−1407 (12)	0.45 (0.02)	Garaga et al. [6]
g-TeO_2	1570 (10)	−1260 (45)	0.5 (0.01)	Garaga et al. [6]
g-TeO_2	1477	−1285	0.74	Sakida et al. [14]
g-TeO_2, TeO_4	1518 (10)	−1215 (30)	0.5 (0.03)	Present Study
g-TeO_2, TeO_3	1705 (10)	−1032 (50)	0.3 (0.05)	Present Study

CSA parameters are in between that of α-TeO_2 and γ-TeO_2, with Δ being closer to that of α-TeO_2 and η being closer to that of γ-TeO_2 (Table 1). Based on these chemical shift parameters and on what is known about the local Te environments in the two crystalline TeO_2 phases, we argue that this TeO_4 environment in the glass is more akin to that in γ-TeO_2 in which all the Te-O bond lengths are dissimilar and, as reflected in its η value, the environment likely includes one Te-O bond that is somewhat longer than the others. In comparison with the major component, the minor component at 1705 ppm is characterized by lower Δ and η. These CSA parameters $\Delta = -1032$ ppm and $\eta = 0.3$ fall in the range expected for either the TeO_3 trigonal pyramid or the distorted trigonal bipyramidal TeO_{3+1} environment that are characteristic of a wide range of tellurite crystals [13]. For example, the TeO_{3+1} environment in the $MgTe_2O_5$ crystal is characterized by: $\delta_{iso} = 1669$ ppm, $\Delta = -1130$ ppm and $\eta = 0.29$. This trigonal bipyramidal Te-O environment in the structure of $MgTe_2O_5$ (Fig. 1) consists of three short Te-O bonds (1.85, 1.86, and 1.97 Å) and one long bond (2.40 Å) [28]. The similarity of the three short Te-O bond lengths and of the three O-Te-O angles in the TeO_{3+1} coordination polyhedra in $MgTe_2O_5$ result in an increased spherical and axial symmetry of the chemical shift tensor at the Te site, compared to that for the Te sites in trigonal bipyramidal TeO_4 environments. Therefore, considering the similarity in the chemical shift parameters between that of the minor component in glassy TeO_2 and of the TeO_{3+1} environment in the $MgTe_2O_5$ crystal, it is quite likely that the former indeed corresponds to TeO_{3+1} environment in the glass. In fact, the presence of long Te-O_{ax} distances characteristic of TeO_{3+1} environments have previously been inferred from comparing the ^{17}O NMR chemical shift of glassy TeO_2 to that of $K_2Te_4O_9$ which has Te-O_{ax} bond lengths upward of 2.5 Å. It has been argued that the bond strength of these long bonds is large enough to be considered a formal bond, albeit weak [6].

On the other hand, the ^{125}Te δ_{iso} range for this minor glassy component covers the δ_{iso} range observed for TeO_3 units in tellurite crystals. The fact that the δ_{iso} distribution for this peak extends to higher frequencies well beyond the range characteristic of TeO_{3+1} (1599–1679 ppm) reported for tellurite crystals is a strong indication that it may represent TeO_3-like environment in TeO_2 glass. It is not clear at this time whether these units are distinctly of the $Te(=O)O_{2/2}$ variety that contain a terminal oxygen or whether they are TeO_{3+1} units with one rather long Te-O_{ax} distance. Garaga et al. has pointed out that the ^{17}O NMR spectrum of TeO_2 glass is somewhat inconsistent with the presence of a terminal oxygen atom in the coordination environment of Te [6]. However, the small fraction (~11%) of this Te environment in TeO_2 glass as determined in this study would predict that only ~5–6% of the oxygen atoms would be of the terminal type, which may go undetected in ^{17}O NMR. It is important to note that if the coordination number for Te in the minor Te-O environment is taken to be 3, then the relative fractions of the major and minor glassy resonances corresponding, respectively, to TeO_4 and TeO_3 environments as obtained from the simulation of the isotropic ^{125}Te line shape shown in Fig. 9, yield an average coordination number $n_{TeO} \approx 3.9$ for glassy TeO_2. This coordination number is higher than the previous estimates of n_{TeO} obtained from neutron diffraction and molecular dynamics simulations using a Te-O nearest-neighbor coordination shell cut off distance of 2.36–2.46 Å [4,20,21].

It may be argued that the significant change in Δ on the low-frequency side of 1400 ppm (Fig. 7) warrants the incorporation of an additional peak in the spectral fitting in this region. An example of such a fit is shown in Fig. 10 and the resulting residual is compared with that obtained from the fit in Fig. 9. Although the quality of the fit is somewhat improved on incorporation of the low-frequency peak, its isotropic shift centered near 1350 ppm does not correspond to any known Te environment in crystalline tellurites. Therefore, it is perhaps more reasonable to consider that the change in Δ near the low-frequency tail is simply a result of the local variation in the distortion of the same TeO_4 trigonal bipyramidal environment. It is worth noting here that a recent study by Garaga et al. [29] has established an approximately linear correlation between the ^{125}Te δ_{iso} and the Te-O coordination number in tellurites. According to this correlation the

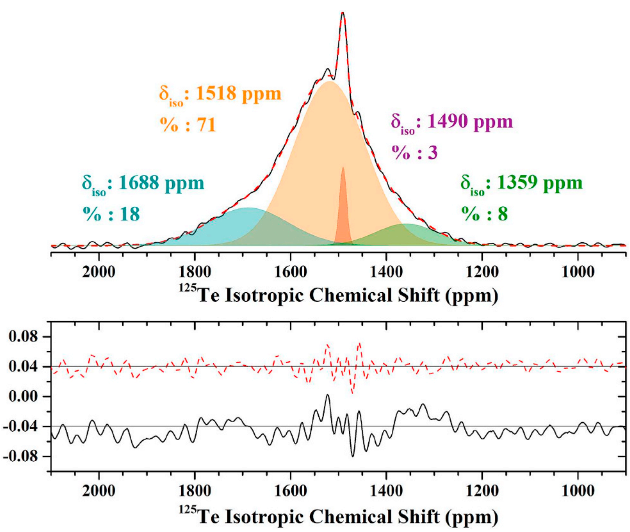

Fig. 10. Top: Simulation of ^{125}Te isotropic NMR spectrum of glassy TeO_2 with 3 glassy environments. Bottom: comparison between the residuals of fits with 2 and 3 glassy environments, shown as solid and dashed lines, respectively.

isotropic shifts of five and six- coordinated Te are in the range of ~1120 and 750 ppm, respectively. Therefore, it is clear that the isotropic ^{125}Te NMR spectrum in Fig. 9a does not provide any indication of the presence of significant concentration of such high-coordinated Te species in TeO_2 glass (Fig. 9).

The sharp resonance at 1491 ppm, corresponding to the Te environment in the crystal phase, is most notable by the abrupt changes in both Δ and η relative to the local trend for the glassy environments (Figs. 7 and 8). Despite the relatively small fraction of the crystalline component (vide infra), the Δ and η for the corresponding Te environment with $\delta_{iso} = 1491$ ppm can be obtained with reasonable accuracy and are found to be -1263 ± 20 ppm and 0.47 ± 0.03, respectively (Fig. 8). These δ_{iso}, Δ, and η values for the crystalline Te environment are all similar to that reported for γ-TeO_2 ($\delta_{iso} = 1500$ ppm; $\Delta = -1410$ ppm, and $\eta = 0.45$) [6]. The slightly lower Δ of the crystalline environment compared to that reported in the literature for γ-TeO_2 is likely due to the fact that the anisotropic slice at this δ_{iso} in the ^{125}Te NMR spectrum in Fig. 5 is a superposition of both the crystalline and the glassy components [6]. The presence of the crystalline γ-TeO_2 in small amount in the glass sample is not surprising as it has been noted previously that the γ phase nucleates first upon slow heating of glassy TeO_2 and at higher temperatures the γ phase transforms into α-TeO_2 [9,10]. The crystalline component constitutes only ~3% of the glassy TeO_2 sample (Fig. 9). This low crystal fraction is consistent with the absence of any indication of crystallinity in the XRD powder pattern and the Raman spectrum of this sample (Figs. 3 and 4). This result also serves to show the relative sensitivity of the 2D ^{125}Te NMR technique to the presence of a small fraction of crystalline component in a glass.

4. Conclusions

The ^{125}Te *pj*MATPASS/CPMG NMR spectrum indicates the possible presence of two distinct Te-O coordination environments in glassy TeO_2. Detailed analysis of the NMR data suggests that ~89% of the Te atoms are present in a trigonal bipyramidal TeO_4 environment, similar to that found in crystalline γ-TeO_2. The ^{125}Te NMR parameters of the second Te site are consistent with either a TeO_3 environment of the type $Te(=O)O_{2/2}$ with a terminal oxygen or, a TeO_{3+1} environment. Here we assign the second Te site to a TeO_3 environment. Approximately 11% of the Te atoms are present in this environment in TeO_2 glass. The resulting average Te-O coordination number of ≈ 3.9 is somewhat higher than those reported in previous studies based on neutron diffraction and molecular dynamics simulation.

Declaration of interests

The authors declare that they have no known competing financial interests or personal relationships that could have appeared to influence the work reported in this paper.

Acknowledgements

This work was supported by grants from the National Science Foundation (NSF-DMR 1505185) to SS and (NSF-DMR 1746230) to SF. The National High Magnetic Field Laboratory is supported by National Science Foundation through NSF DMR-1157490, DMR-1644779, and the State of Florida. MATM acknowledges support from Lawrence Livermore National Laboratory under contract DE-AC52-07NA27344.

References

[1] R.A.H. El-Mallawany, Tellurite Glasses Handbook: Physical Properties and Data, Second ed., CRC Press, 2016.
[2] M. Smirnov, A. Mirgorodsky, O. Masson, P. Thomas, Quantum mechanical study of pre-dissociation enhancement of linear and nonlinear polarizabilities of $(TeO_2)_n$ oligomers as a key to understanding the remarkable dielectric properties of TeO_2 glasses, J. Phys. Chem. A 116 (2012) 9361–9369.
[3] A.P. Mirgorodsky, M. Soulis, P. Thomas, T. Merle-Méjean, *Ab initio* study of nonlinear optical susceptibility of TeO_2-based glasses, Phys. Rev. B 73 (2006) 134206.
[4] E.R. Barney, A.C. Hannon, D. Holland, N. Umesaki, M. Tatsumisago, R.G. Orman, S. Feller, Terminal oxygens in amorphous TeO_2, J. Phys. Chem. Lett. 4 (2013) 2312–2316.
[5] N.S. Tagiara, D. Palles, E.D. Simandiras, V. Psycharis, A. Kyritsis, E.I. Kamitsos, Synthesis, thermal and structural properties of pure TeO_2 glass and zinc-tellurite glasses, J. Non-Cryst. Solids 457 (2017) 116–125.
[6] M.N. Garaga, U. Werner-Zwanziger, J.W. Zwanziger, A. DeCeanne, B. Hauke, K. Bozer, S. Feller, Short-range structure of TeO_2 glass, J. Phys. Chem. C 121 (2017) 28117–28124.
[7] P.A. Thomas, The crystal tructure and absolute optical chirality of paratellurite α-TeO_2, J. Phys. C Solid State Phys. 21 (1988) 4611–4627.
[8] J.C. Champarnaud-Mesjard, S. Blanchandin, P. Thomas, A. Mirgorodsky, T. Merle-Méjean, B. Frit, Crystal structure, Raman spectrum and lattice dynamics of a new metastable form of tellurium dioxide: γ-TeO_2, J. Phys. Chem. Solids 61 (2000) 1499–1507.
[9] A.G. Kalampounias, G. Tsilomelekis, S. Boghosian, Glass-forming ability of TeO_2 and temperature induced changes on the structure of the glassy, supercooled, and molten states, J. Chem. Phys. 142 (2015) 154503.
[10] O. Noguera, T. Merle-Méjean, A.P. Mirgorodsky, M.B. Smirnov, P. Thomas, J.-C. Champarnaud-Mesjard, Vibrational and structural properties of glass and crystalline phases of TeO_2, J. Non-Cryst. Solids 330 (2003) 50–60.
[11] S. Sakida, S. Hayakawa, T. Yoko, ^{125}Te NMR study of MO-TeO_2 (M = mg, Zn, Sr, Ba and Pb) glasses, J. Ceram. Soc. Jpn. 107 (1999) 395–402.
[12] J.C. McLaughlin, S.L. Tagg, J.W. Zwanziger, D.R. Haeffner, S.D. Shastri, The structure of tellurite glass: a combined NMR, neutron diffraction, and X-ray diffraction study, J. Non-Cryst. Solids 274 (2000) 1–8.
[13] S. Sakida, S. Hayakawa, T. Yoko, Part 1. ^{125}Te NMR study of tellurite crystals, J. Non-Cryst. Solids 243 (1999) 1–12.
[14] S. Sakida, S. Hayakawa, T. Yoko, Part 2. ^{125}Te NMR study of M_2O-TeO_2 (M = li, Na, K, Rb and Cs) glasses, J. Non-Cryst. Solids 243 (1999) 13–25.
[15] J.C. McLaughlin, S.L. Tagg, J.W. Zwanziger, The structure of alkali tellurite glasses, J. Phys. Chem. B 105 (2001) 67–75.
[16] E.R. Barney, A.C. Hannon, D. Holland, N. Umesaki, M. Tatsumisago, Alkali environments in tellurite glasses, J. Non-Cryst. Solids 414 (2015) 33–41.
[17] U. Hoppe, I. Gugov, H. Bürger, P. Jóvári, A.C. Hannon, Structure of tellurite glasses - effects of K_2O or P_2O_5 additions studied by diffraction, J. Phys. Condens. Matter 17 (2005) 2365–2386.
[18] Z. Whittles, M. Marple, I. Hung, Z. Gan, S. Sen, Structure of BaO-TeO_2 glasses: a two-dimensional ^{125}Te NMR spectroscopic study, J. Non-Cryst. Solids 481 (2018) 282–288.
[19] S. Sakida, S. Hayakawa, T. Yoko, ^{125}Te and ^{51}V static NMR study of V_2O_5-TeO_2 glasses, J. Phys. Condens. Matter 2000 (2000) 2579–2595.
[20] A. Gulenko, O. Masson, A. Berghout, D. Hamani, P. Thomas, Atomistic simulations of TeO_2-based glasses: interatomic potentials and molecular dynamics, Phys. Chem. Chem. Phys. 16 (2014) 14150–14160.
[21] F. Pietrucci, S. Caravati, M. Bernasconi, TeO_2 glass properties from first principles, Phys. Rev. B 78 (2008) 064203.
[22] D.C. Kaseman, I. Hung, K. Lee, K. Kovnir, Z. Gan, B. Aitken, S. Sen, Tellurium speciation, connectivity, and chemical order in As_xTe_{100-x} glasses: results from two-dimensional ^{125}Te NMR spectroscopy, J. Phys. Chem. B 119 (2015) 2081–2088.
[23] R.K.B. Harris, E. D, S.M.C. De Menezes, R. Goodfellow, P. Granger, NMR nomenclature. Nuclear spin properties and conventions for chemical shifts(IUPAC

recommendations 2001), Pure Appl. Chem. 73 (2001) 1795.
[24] D. Massiot, F. Fayon, M. Capron, I. King, S. Le Calvé, B. Alonso, J.-O. Durand, B. Bujoli, Z. Gan, G. Hoatson, Modelling one- and two-dimensional solid-state NMR spectra, Magn. Reson. Chem. 40 (2002) 70–76.
[25] M. Mehring, Principles of High Resolution NMR in Solids, Springer-Verlag, Berlin, 1983.
[26] A. DeCeanne, et al., Producing amorphous tellurium dioxide, 12th Pacific Rim Conference on Ceramic and Glass Technology (PACRIM 12), Poster Presentation, Waikoloa, Hawaii, USA, 2017.
[27] A.G. Kalampounias, S. Boghosian, Distribution of tellurite polymorphs in the xM_2O-$(1\text{-}x)TeO_2$ (M = Li, Na, K, Cs, and Rb) binary glasses using Raman spectroscopy, Vib. Spectrosc. 59 (2012) 18–22.
[28] M. Weil, Redetermination of $MgTe_2O_5$, Acta Crystallogr. Sect. E: Struct. Rep. Online 61 (2005) i237–i239.
[29] M.N. Garaga, U. Werner-Zwanziger, J.W. Zwanziger, Inorg. Chem. 57 (2018) 892–898.